ADVANCED HEALTHCARE MATERIALS
www.advhealthmat.de

Engineering Extracellular Matrix-Bound Nanovesicles Secreted by Three-Dimensional Human Mesenchymal Stem Cells

*Chang Liu, Xingchi Chen, Yuan Liu, Li Sun, Zhibin Yu, Yi Ren, Changchun Zeng, and Yan Li**

Extracellular matrix (ECM) in the human tissue contains vesicles, which are defined as matrix-bound nanovesicles (MBVs). MBVs serve as one of the functional components in ECM, recapitulating part of the regulatory roles and in vivo microenvironment. In this study, extracellular vesicles from culture supernatants (SuEVs) and MBVs are isolated from the conditioned medium or ECM, respectively, of 3D human mesenchymal stem cells. Nanoparticle tracking analysis shows that MBVs are smaller than SuEVs (100–150 nm). Transmission electron microscopy captures the typical cup shape morphology for both SuEVs and MBVs. Western blot reveals that MBVs have low detection of some SuEV markers such as syntenin-1. miRNA analysis of MBVs shows that 3D microenvironment enhances the expression of miRNAs such as miR-19a and miR-21. In vitro functional analysis shows that MBVs can facilitate human pluripotent stem cell-derived forebrain organoid recovery after starvation and promote high passage fibroblast proliferation. In macrophage polarization, 2D MBVs tend to suppress the pro-inflammatory cytokine IL-12β, while 3D MBVs tend to enhance the anti-inflammatory cytokine IL-10. This study has the significance in advancing the understanding of the bio-interface of nanovesicles with human tissue and the design of cell-free therapy for treating neurological disorders such as ischemic stroke.

1. Introduction

Human mesenchymal stem cells (hMSCs) are multipotent stem cells capable of self-renewal and of differentiation into other tissues.[1] They have attracted great interest as novel medical treatments recently. More than 1138 clinical trials using hMSCs as therapeutic agents were registered at ClinicalTrials.gov by June 2020.[2] Though hundreds of trials have shown its safety, the clinical development of hMSC therapy has advanced slowly.[3,4] The number of cells required (dozens to hundreds of millions of cells per patient per dose) is one of the obstacles that have yet to overcome.[3] Besides, their usefulness as a cell pharmaceutical agent is significantly influenced by the biological fitness of hMSCs and their functionalities.[3,5]

hMSCs act by direct contact with host cells to modulate their functions, or differentiation into specific cell lineages and integration into tissues.[6] Since the discovery that the therapeutic ability of conditioned medium from hMSCs was effective,[7] another mechanism—secretion of secretome that assists cell repair and growth—was discovered. One of the bioactive components in the secretome is extracellular vesicles (EVs), with the small size subpopulation known as exosomes (30–150 nm), the lipid membrane-enclosed vesicles secreted from all cell types. EVs carry a variety of cargo, including proteins, peptides, lipids, carbohydrates, DNA, mRNA, microRNA (miRNA), and long non-coding RNA, and capture the native characteristics of source cells.[8] hMSC-EVs are capable of reducing myocardial

C. Liu, X. Chen, Y. Liu, L. Sun, Y. Li
Department of Chemical and Biomedical Engineering
FAMU-FSU College of Engineering
Florida State University
Tallahassee, FL 32310, USA
E-mail: yli4@fsu.edu

X. Chen, Z. Yu, C. Zeng
High Performance Materials Institute
FAMU-FSU College of Engineering
Florida State University
Tallahassee, FL 32310, USA

L. Sun, Y. Ren
Department of Biomedical Sciences
College of Medicine
Florida State University
Tallahassee, FL 32306, USA

Z. Yu, C. Zeng
Department of Industrial and Manufacturing Engineering
FAMU-FSU College of Engineering
Florida State University
Tallahassee, FL 32310, USA

The ORCID identification number(s) for the author(s) of this article can be found under https://doi.org/10.1002/adhm.202301112

DOI: 10.1002/adhm.202301112

ischemia/reperfusion injury, promoting cardiac endothelial microvascular regeneration, suppressing myofibroblast differentiation, accelerating skeletal muscle regeneration, etc.[9,10] As therapeutic reagents, EVs have several advantages over hMSCs: 1) they do not replicate so there is a lower possibility of developing into cancerous cells; 2) they do not cause an immune response so immunosuppression is not necessary; 3) they have small sizes, therefore the risk of elimination in the vasculature is less and they can easily distribute to other tissues and pass the blood-brain barrier; 4) they can be generated at a high yield of 10^4–10^6 particles/cell.[8,11,12] These benefits make EVs a promising alternative for hMSC therapy.

In most studies, EVs were isolated from cell culture conditioned media or bio-fluids, such as blood and urine.[13] However, in 2016, a study reported that similar vesicles can be isolated from extracellular matrix (ECM).[14] These vesicles were named matrix-bound nanovesicles (MBVs), and recognized as a crucial and functional element of ECM. When ECM was used for surgical reconstruction, it interacted with host cells, enhanced cellular proliferation, differentiation, and migration, promoted angiogenesis, modulated immune response, etc.[15] Although it is not proven that MBVs mediate all of the physiological effects attributed to ECM, it has been suggested that MBVs recapitulated some of the biologic effects of the parent ECM.[14]

Functionally, MBVs from porcine urinary bladder matrix (UBM) showed the ability of inducing the M2 phenotype of macrophages and promoting the neurite extension of neuroblastoma cells.[14,16,17] In an in vivo study, intravitreal UBM-MBV injections mitigated intraocular pressure-induced retinal ganglion cells axon degeneration and death, protected the axon connectivity to visual nuclei in the brain, and prevented loss in retinal function.[18] Besides, UBM-MBVs delivered via intravenous or peri-articular injection to rats attenuated acute and chronic pristane-induced rheumatoid arthritis by modulating local synovial macrophages and systemic myeloid populations.[19] In addition, porcine vocal fold lamina propria-derived MBVs together with macromolecules downregulated the smooth muscle actin *ACTA2* expression under transforming growth factor-beta 1 stimulation.[20] In a more recent study, MBVs were isolated from human left ventricles ECM of young or aged men and women, and the data indicated that synergistic effects of miRNAs from matrix-resident exosomes may influence the differential clinical response to myocardial infarction.[21]

However, most studies generated MBVs from animal or human tissues. Human tissues are a limited resource, while animal-derived MBVs raise safety concerns for clinical purposes.[22] All these make in vitro human stem cell cultures, including monolayers and 3D spheroids or organoids, promising replacement for tissue-derived MBVs. In our previous work, EVs from culture supernatants (SuEVs) were isolated from 2D and 3D hMSCs, and were characterized via proteomics and in vitro models.[11,23] In this study, 2D and 3D hMSCs were generated, and their small RNAs were sequenced. The SuEVs and MBVs were isolated from 2D normoxia, 2D hypoxia, 3D culture conditioned media, and decellularized ECM, respectively. Since 3D aggregates may have oxygen transport limitation toward the core, they were mainly cultured under normoxia condition. The enhanced cell–cell interactions in 3D hMSC aggregates and the re-configured metabolism and primitive properties make them attractive for therapeutic applications.[24–26] The decellularization process and MBV release were characterized. Then, SuEVs and MBVs were compared in terms of size, concentration (or yield), typical exosomal markers, and morphology. Since our previous study thoroughly compared 2D and 3D SuEVs,[11,23] this study focused on 2D and 3D MBVs. Due to the resemblance of 2D normoxia culture and 2D hypoxia culture, the 2D normoxia condition was kept for further analysis along with 3D condition, such as miRNA cargo expression. The functions of 2D and 3D MBVs were investigated through several in vitro culture models, including starvation model, wound healing model, proliferation model, as well as immunomodulation model. This study paved the way for understanding the bio-interface of SuEVs and MBVs with the human tissue and the design of cell-free based therapy for treating neurological disorders such as Alzheimer's disease and ischemic stroke.

2. Results

2.1. Characterizations of 3D hMSC Culture and Decellularization Process

The procedure to generate 3D hMSCs using dynamic wave motion culture was illustrated in **Figure 1**A. P4 or P5 hMSCs were passaged and seeded as 2D monolayer cultures (normoxia and hypoxia) or 3D aggregates. The characteristics of 2D and 3D hMSC aggregates been characterized in our previous studies using proteomics and transcriptome analysis.[11,23] The small RNA sequencing of 2D and 3D hMSCs demonstrated distinct profiles of miRNAs and piRNAs. Principle component analysis showed two clear clusters of 2D and 3D cultures (Figure 1B). Volcano plot exhibited a total of 98 differentially expressed genes (DEGs) with 13 significantly downregulated DEGs (e.g., miR-486), 3 significantly upregulated DEGs (e.g., miR-21), and 82 insignificantly DEGs in 3D samples comparing to 2D samples (FDR < 0.05, Log2 fold change > 1.0) (Figure 1C and Table S5, Supporting Information). Moreover, the expression level of the significantly expressed DEGs also showed considerable difference in the heatmap (Figure 1D). Kyoto Encyclopedia of Genes and Genomes (KEGG) (Figure 1E,F) and Gene Ontology (GO) (Figure 1G–I) enrichment analysis indicated the signaling pathways (e.g., longevity regulating pathway and TGF-beta signaling pathway) and the gene functions that the mRNA targets of DEGs participated in. DAG figures also showed the hierarchical relationships among different gene functions in downregulated and upregulated miRNA-targeted mRNAs (Figures S1–S4, Supporting Information).

The conditioned media of the 2D and 3D cultures were collected to isolate SuEVs. The cells were decellularized to harvest MBVs from the ECM (**Figure 2**A). 2D hMSCs were spindle-shaped, while 3D hMSCs formed aggregates with diameters of 100–200 μm on day 2 (Figure 2B). Decellularization was performed by adding 0.5% Triton X-100 for 5 min, and it removed 40–50% nuclei for 2D normoxia culture (Figure 2C,D). Further treated with DNase I resulted in less than 10% nuclei. After decellularization, ECM components were examined. The decellularized hMSC ECM was rich in laminin and collagen I. Though efficient for 2D culture, DNase I was less efficient in reducing nuclei of 3D aggregates, which had ≈25% nuclei left (Figure 2E).

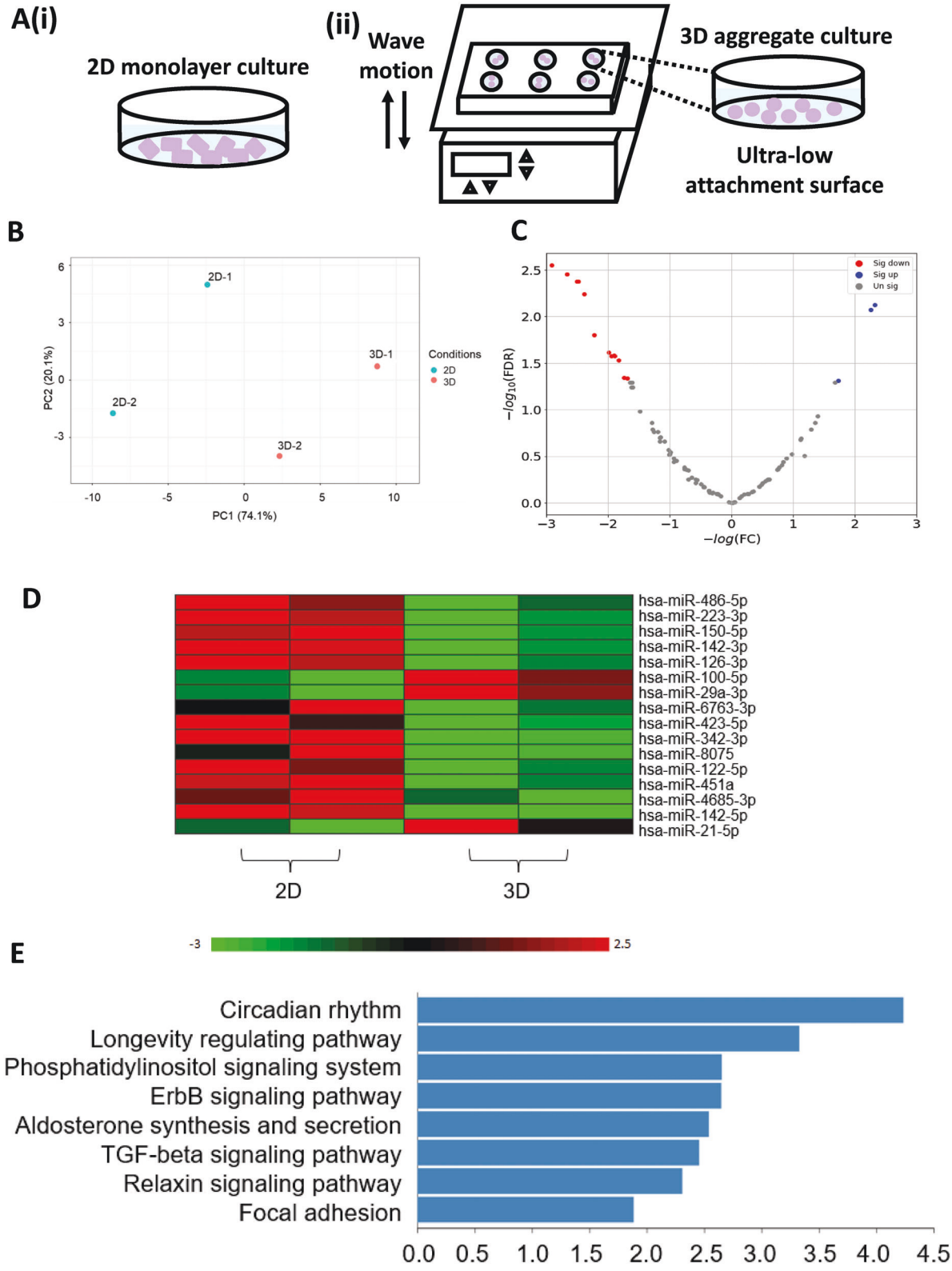

Figure 1. miRNA sequencing of two-dimensional (2D) and three-dimensional (3D) human mesenchymal stem cells (hMSCs). A) 2D and 3D hMSC culture illustration. B) Principal Component Analysis (PCA) of 2D and 3D cells. C) Volcano plot. D) Heatmap of differentially expressed miRNAs. E) Downregulated miRNAs targeted mRNA participated signaling pathways enriched in KEGG analysis. F) Upregulated miRNAs targeted mRNA participated signaling pathways enriched in KEGG analysis. GO analysis of G) biological process, H) cellular component, and I) molecular function: (left) downregulated miRNAs targeted mRNAs, (right) upregulated miRNAs targeted mRNAs.

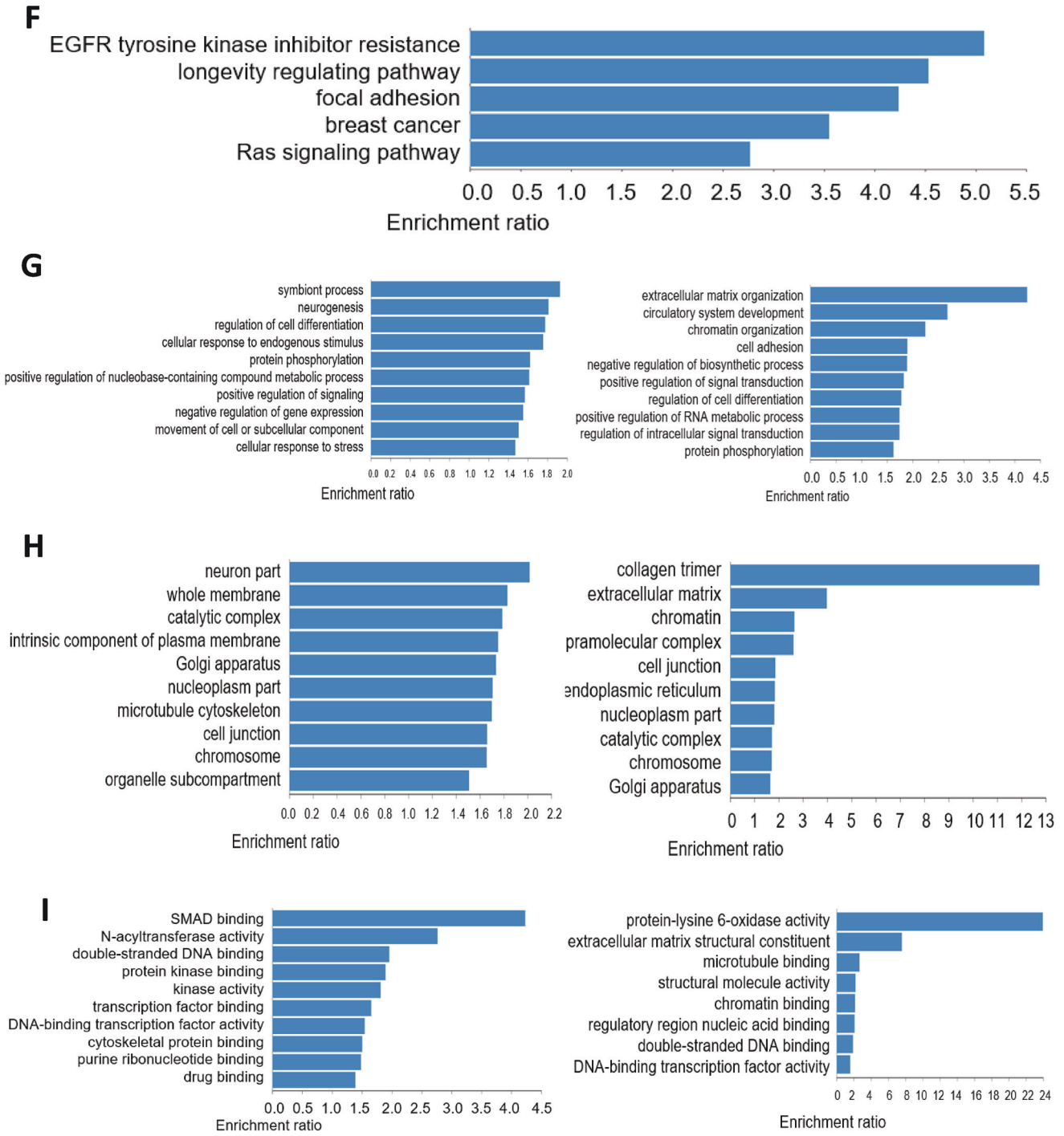

Figure 1. *Continued*

2.2. Characterizations of SuEVs and MBVs

To determine whether MBVs released from ECM were affected by enzyme treatment, three releasing conditions were tested: 0.01 mg mL^{-1} proteinase K, 0.01 mg mL^{-1} collagenase, and the no enzyme solution (**Figure 3**A,B). There were no statistically significant differences for different treatment groups; however, the purities were the highest for both 2D and 3D MBVs when treated with proteinase K.

Size distributions of SuEVs and MBVs were determined by nanoparticle tracking analysis (NTA) (Figure 3C). For mean size, 2D SuEVs were larger than 2D MBVs (≈180 nm vs ≈150 nm). Mode size showed a similar trend (≈150 nm vs 100–120 nm) (Figure 3D). 2D MBVs were smaller than 3D MBVs (≈150 nm

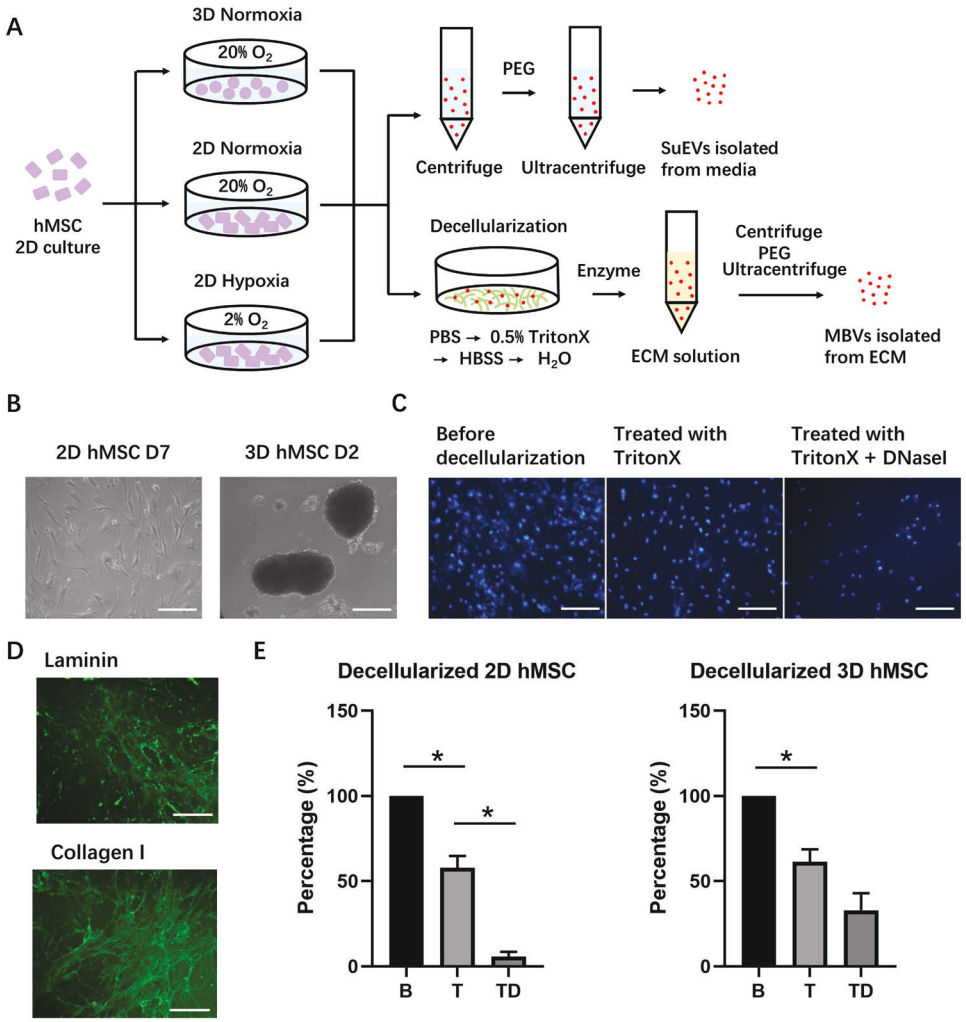

Figure 2. Schematic illustration of culture condition, decellularization, as well as extracellular vesicles (EVs) from culture supernatants (SuEV) and matrix-bound nanovesicles (MBV) isolation. A) 2D hMSC cultures were divided into three groups: 3D normoxia culture, 2D normoxia culture, and 2D hypoxia culture. For SuEV isolation, the conditioned media underwent serial centrifuges and finally an ultracentrifuge step. For MBV isolation, there was a decellularization step to harvest ECM solutions, which was achieved by the treatment of 0.5% Triton X-100, then the ECM solutions went through the same process as SuEV isolation. B) Morphology of 2D and 3D hMSCs. C) Cells decellularized with Triton X-100 and/or DNase I. D) Two ECM components—Laminin and Collagen I—imaging after decellularization. E) Percentages of remaining DNA of 2D and 3D hMSCs after decellularization. Scale bar: 100 μm. B: before decellularization; T: treated with Triton X; TD: treated with Triton X and DNase I.

vs ≈190 nm) for mean size. For mode size, there was no significant difference. Comparing the yields of MBVs, both 2D and 3D hMSC culture generated one order magnitude higher SuEVs per cell than MBVs per cell (Figure 3E). Within the SuEV groups, 2D normoxia culture and 3D aggregates were more productive than the 2D hypoxia culture. While for the MBV groups, the 3D culture exhibited higher productivity than the 2D cultures. Similar to the yields, the purities of SuEVs were much higher than MBVs (Figure 3F). And in both SuEV groups and MBV groups, the 3D groups showed higher purities than the 2D groups.

Several exosomal markers were examined by western blot (**Figure 4**A). Calnexin is a marker that is abundant in cell lysate but should not exist in SuEVs and MBVs. Other markers, HRS, HSC70, Syntenin-1, and CD81 showed high expression in SuEVs as expected. However, some of these markers (HRS and HSC70) were not detected in MBVs, and some of the markers (CD81 and Syntenin-1) had low abundance compared to the SuEVs. To confirm the existence of MBVs, transmission electron microscopy (TEM) was performed (Figure 4B). MBVs from both 2D cultures and 3D aggregates were typical round cup-shaped double layered nanoparticles, similar to the morphology of SuEVs.

To study the miRNA cargo in MBVs, miRNA reverse transcription polymerase chain reaction (RT-PCR) was performed on several miRNAs which were selected based on our previous studies[23,27] and our intended future studies related to neurological disorders such as ischemic stroke. miR-10 and miR-19a are angiogenesis-related, and were highly expressed in 3D MBVs compared to 2D MBVs (Figure 4C[i]). miR-21 and miR-22 are cytoskeleton-related, and were significantly elevated in 3D MBVs compared to 2D MBVs as well (Figure 4C[ii]). Especially the miR-21 was ≈55-fold higher in 3D MBVs than in 2D MBVs, while in cells, it was only 1.7-fold. miR-125b and miR-145 are

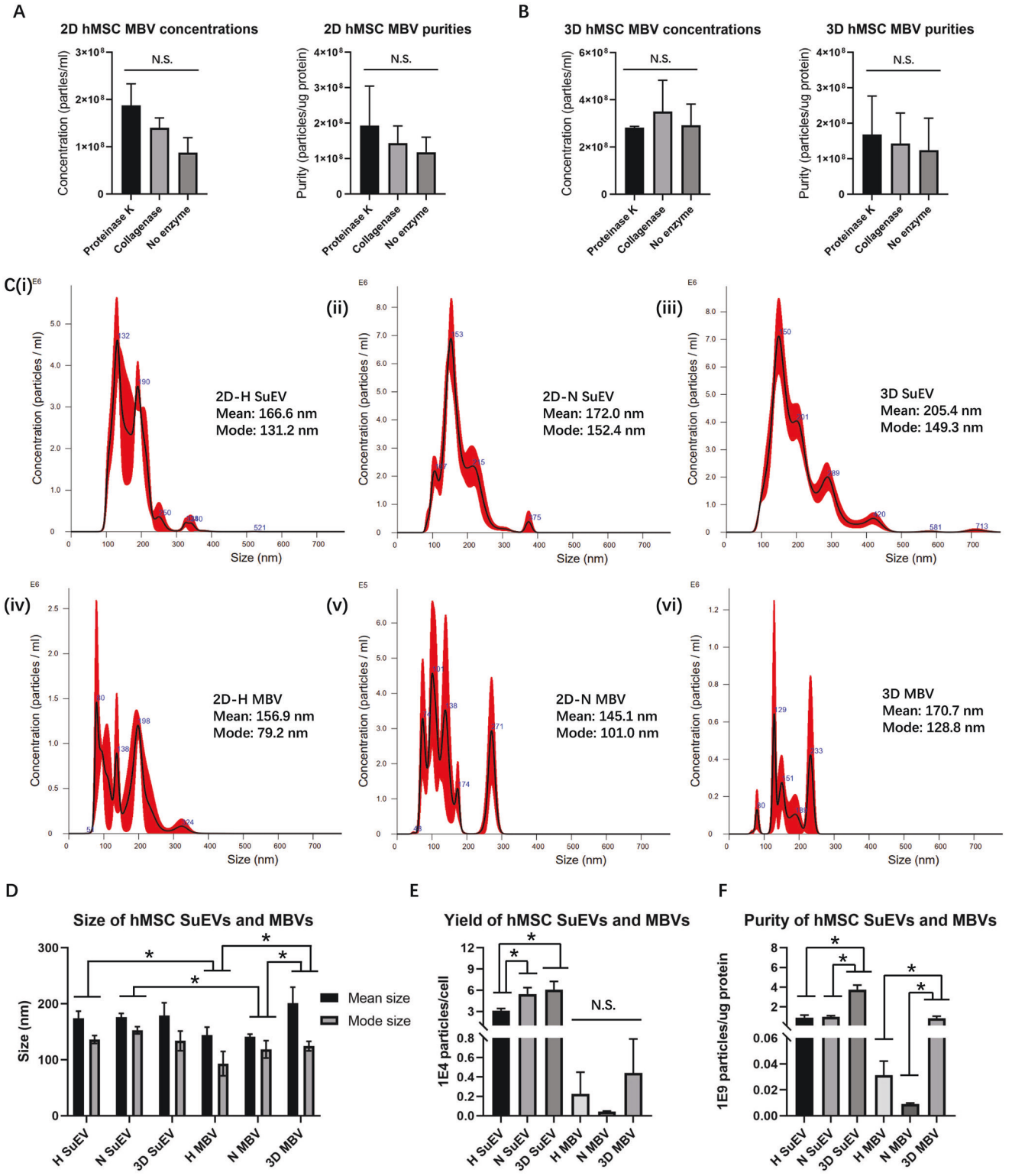

Figure 3. 2D and 3D hMSC SuEV and MBV quantitative characterization. A,B) MBVs released by different enzymes (Proteinase K, Collagenase, and no enzyme): A) Concentrations and purities of 2D hMSC MBVs; B) Concentrations and purities of 3D hMSC MBVs. C) Representative size distribution of SuEVs and MBVs measured by nanoparticle tracking analysis (NTA). D) Mean and mode sizes of SuEVs and MBVs. 2D SuEVs were larger than 2D MBVs, 2D MBVs were smaller than 3D MBVs. E,F) Yields and purities of SuEVs and MBVs. $n = 3$. H: hypoxia; N: normoxia. * indicates $p < 0.05$.

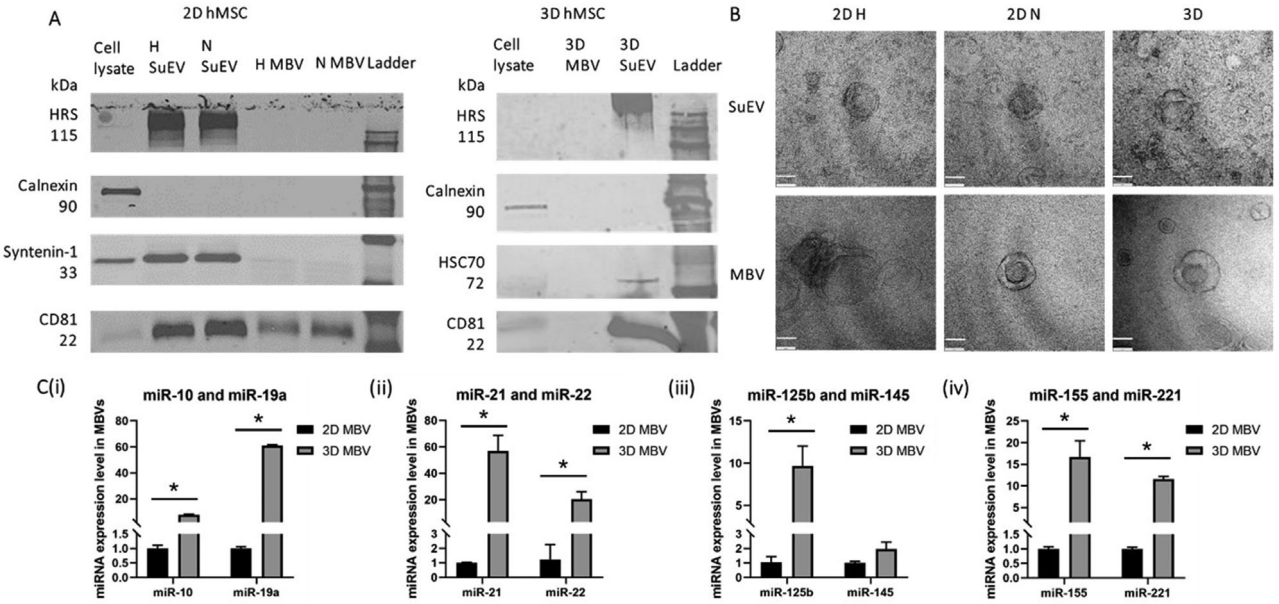

Figure 4. Western blot and transmission electron microscopy, and miRNA cargo analysis of 2D and 3D MBVs. A) Western blot of SuEVs and MBVs. Calnexin is a negative exosomal marker that was abundant in cells, other markers were abundant in exosomes. All the SuEVs showed typical exosomal markers, while MBVs were absent or low at these markers. B) TEM imaging demonstrated that SuEVs and MBVs had the typical double layered cup-shape morphology of exosomes. Scale bar: 60 μm. C) Reverse transcription-polymerase chain reaction (RT-PCR) analysis of miRNA in MBVs. (i) Angiogenic and cell proliferation related miR-10 and miR-19a were highly expressed in 3D MBVs. (ii) Cytoskeleton related miR-21 and miR-22 were highly expressed in 3D MBVs. (iii) ECM abundant miR-125b and miR-145 showed higher expression in 3D MBVs. (iv) Wnt signaling related miR-155 and miR-221 were highly expressed in 3D MBVs. $n = 3$. * indicates $p < 0.05$.

involved in adhesion and plasticity regulation, and only miR-125b exhibited rich abundance in 3D MBVs compared to 2D MBVs (Figure 4C[iii]). miR-155 and miR-221 are involved in regulation of Wnt signaling, and their expression were 10–20-folds higher in 3D MBVs compared to the 2D MBVs (Figure 4C[iv]). Apparently, miRNA cargo in MBVs did not have direct correlation with miRNAs in parent cells as shown in Figure 1.

2.3. In Vitro Functional Analysis and Immunomodulation

To evaluate whether MBVs possess potential therapeutic effects, they were subject to in vitro functional analysis. For the forebrain organoid starvation model, the iNPCos were starved for 8 h and followed by an overnight recovery with or without adding MBVs, and the controls were those iNPCos that were not starved (**Figure 5**A). Results showed that the presence of 3D MBVs slightly enhanced the ratio (≈1.2-fold) of MTT values of 8 h-starved cells to the MTT values of none-starved cells, but 2D MBVs increased the ratio to about 1.5-fold. In the wound healing assay, a scratch was made in each well where fibroblasts grew, and the wound closure was tracked for 16 h. However, neither 2D MBVs nor 3D MBVs had a significant advantage in promoting wound healing compared to the no MBV control (Figure 5B and Figure S5, Supporting Information). In the proliferation assay, cell numbers of P15 (and P9) fibroblasts with or without MBVs were determined every day for 4 days (Figure 5C and Figure S6, Supporting Information). For a better evaluation of the MBV effects, relative percentages of the cell numbers in MBV groups over the control group were calculated. In general, both 2D and 3D MBVs contributed to fibroblast proliferation. However, the 2D MBVs promoted the fibroblast growth continuously throughout the 4-day culture, while the 3D MBVs improved the fibroblast growth for the first 2 days.

The immuno-modulation ability of MBVs was studied by stimulating the macrophage polarization with Aβ42 oligomers and IL-4. After the 24 h-stimulation, the cells were harvested for RT-PCR, and the media were collected for enzyme-linked immunosorbent assay (ELISA). The RT-PCR results showed that Aβ42 treatment greatly increased the expression of TNF-α, and slightly increased the mRNA expression of IL-6 and IL-12β (**Figure 6**A). These three are pro-inflammatory markers, and were reduced by 2D MBVs, especially the IL-12β. For the other three markers IL10, TGF-β, and CD163, which are anti-inflammatory, 3D MBVs showed higher mRNA expression especially for IL-10. Under the IL-4 stimulation, 2D and 3D MBVs did not show much difference in modulating the mRNA expressions of these markers. Several pro-inflammatory cytokines (TNF-α, IL-6, and IL-1β) were measured at a protein level using ELISA (Figure 6B). Interestingly, all the three Aβ42 stimulated groups showed reduced TNF-α cytokine, which was expected to be higher according to the RT-PCR results. However, 2D and 3D MBVs lowered the TNF-α secretion for the IL-4 stimulated groups. For IL-6 and IL-1β, there were no significant differences among different groups.

3. Discussion

In this study, proteinase K, collagenase, or no enzyme solution were evaluated to digest ECM and harvest MBVs. Concerns arise that the reagents used for decellularization and ECM digestion

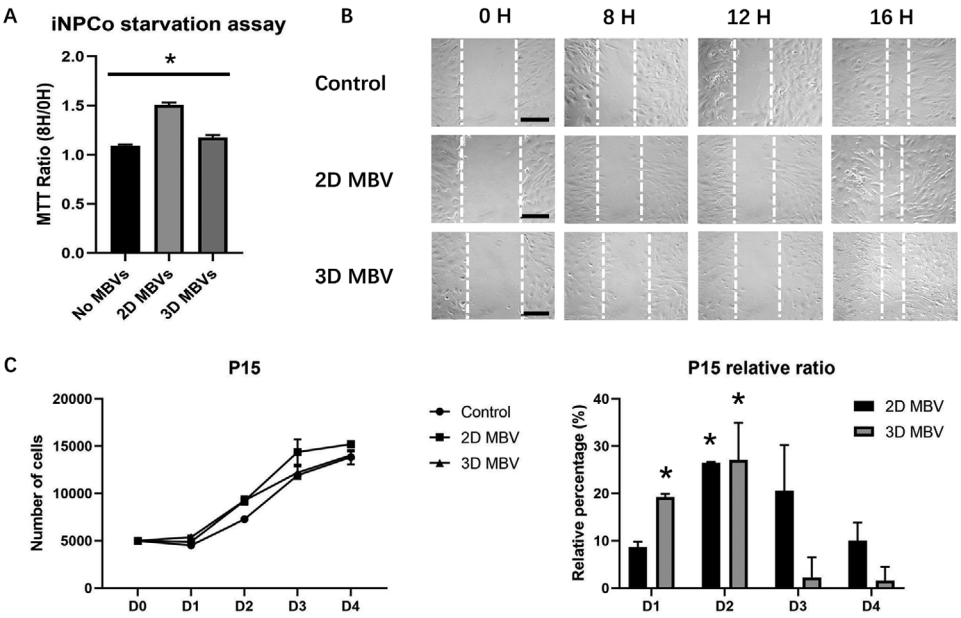

Figure 5. In vitro functional assays for MBVs. A) iNPCo starvation model showed that iNPCo recovered with the addition of MBVs had higher viability after starvation. B) Morphology of wound healing process. In vitro wound healing model of the P15 fibroblasts did not demonstrate the advantage of MBVs in promoting wound healing. C) Proliferation assay indicated that P15 fibroblasts cultured with MBVs had higher (i) cell numbers and (ii) relative percentages than the control. Scale bar: 100 μm. $n = 3$. * indicates $p < 0.05$.

could damage MBVs. However, it is proposed that the close association of MBVs with collagen fibers provides protection from those agents.[14] In addition, MBVs benefit from their nanoscale size plus the inherent stability of EVs, such as resistance to RNase degradation, lyophilization, and extreme changes in temperature and pH.[28] In some studies, MBVs were released from tissue ECM by collagenase or liberase rather than proteinase K.[14,16,18,29] Proteinase K is a stable protease that degrades a broad spectrum of proteins, collagenase is a relatively crude combination of collagenase isoforms breaking the peptide bonds in collagen, and liberase is a highly purified preparation of collagenases I and II.[30] MBVs from UBM-ECM showed lower concentrations when treated with proteinase K than treated with collagenase and liberase, and the MBV purities were similar among all groups.[31] Our 3D MBV results were consistent with previous study,[31] probably due to the resemblance of 3D aggregates and tissues.

Proteinase K could be used for purifying EVs for EV isolation from plasma.[32] However, proteinase K has been previously reported to reduce exosomal surface marker, while the marker insides exosomes was protected from proteinase K.[33] Liberase or collagenase-released MBVs also demonstrated the absence or weakened marker expression by western blot.[14,34] Our results of hMSC MBV exosomal marker expression in this study were consistent with the observations in the literature of other tissue-derived MBVs. However, the amount of enzyme used for treatment may impact the western blot results, and the enzyme remnant may influence MBV functional effects. It was reported that proteinase K can be inhibited by incubation with 5 mM phenylmethylsulfonyl fluoride, and the resulted samples could be used for in vitro macrophage uptake assay and in vivo lung distribution assay,[33] suggesting a way of attenuating the effect of remnant enzymes in MBVs harvesting.

MBVs have similar morphology to SuEVs, but 2D SuEVs were larger than 2D MBVs. This was different from Hussey et al.'s study, which used 3T3 fibroblast culture model.[34] By quantitative comparison, SuEVs exhibited higher yield and purities than MBVs, due to higher particle numbers. Within MBV groups, 3D culture showed higher yield and purities than the 2D cultures, which was consistent with the results of SuEV groups in this study and our previous studies.[11,23] Like SuEVs from different cellular origin have their own unique contents, MBVs from different cells (bone marrow MSCs, adipose MSCs, and umbilical cord MSCs) have unique miRNA cargo.[34] Coming from the same cell source, SuEVs and MBVs possess significant difference in miRNA contents as well.[34] Our study revealed that different culture conditions, monolayer or aggregates, also had influence on miRNA abundance in MBVs, and 3D aggregates tended to enhance miRNA levels in MBVs compared to 2D culture.

miRNA cargo has been recognized as the major contributor to the therapeutic effects of EVs.[35] As a newly discovered population of nanovesicles, MBV functions are partially related to their miRNA cargo as well. In our study, eight miRNAs in MBVs were tested to demonstrate the potential functions of MBVs. miR-10 regulates the angiogenic behavior of human endothelial cells by directly modulating the levels of *mflt1* and its soluble splice isoform *sflt1*, and by directly targeting *mib1*.[36] In an in vivo study, overexpression of miR-10a in aged human bone marrow-MSCs activated protein kinase (Akt) and stimulated the production of angiogenic factors, resulting in increased angiogenesis in myocardial infarcted mouse hearts.[37] miR-19a promotes angiogenesis and proliferation by activating Akt and extracellular-signal regulated kinase and by inhibiting TSP-1, a known suppressor of angiogenesis and proliferation.[38] However, a contradicted study showed that miR-19a inhibited endothelial cells angiogenesis

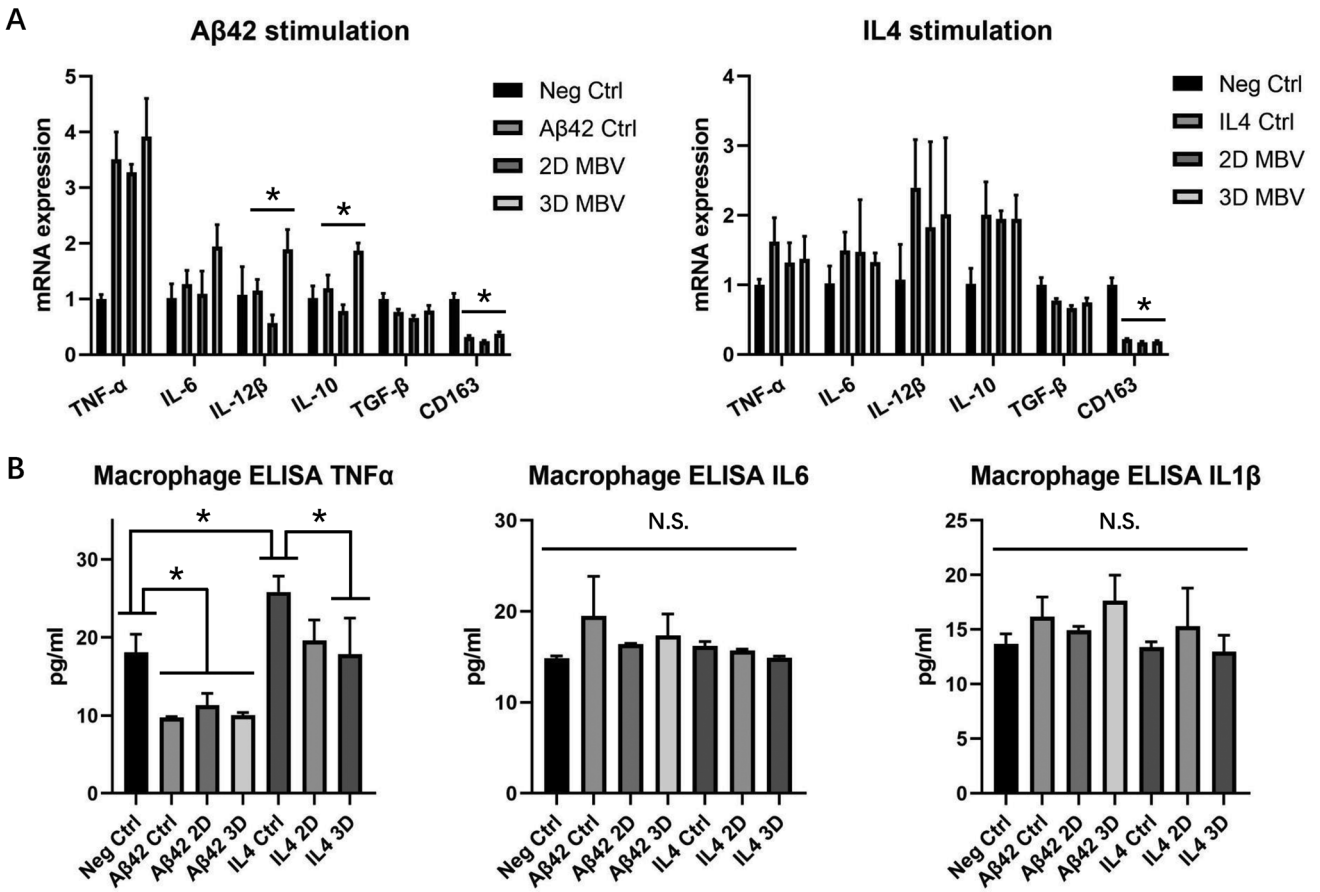

Figure 6. Macrophage immuno-modulation by MBVs. A) The change of mRNA expression for pro-inflammatory and anti-inflammatory markers of macrophages stimulated by Aβ42 and IL-4 and treated with 2D or 3D MBVs. B) ELISA measurements of the cytokines secreted by macrophages stimulated by Aβ42 oligomers and IL-4 along with the treatments of 2D or 3D MBVs ($n = 3$). * indicates $p < 0.05$.

and proliferation and attenuated heart function of mice after myocardial infarction by targeting HIF-1α.[39] miR-21 contributes to angiogenesis as well, and it also regulates cell adhesion, cytoskeleton rearrangement, and ECM reconstitution.[40] When expanding rat MSCs on stiff culture substrates, miR-21 levels were gradually elevated by continuous regulation through the acutely mechanosensitive myocardin-related transcription factor-A, and remained high for more than 2 weeks after removing the mechanical stimulus.[41] Similarly, miR-22 regulated cytoskeleton rearrangement by inhibiting transgelin (an actin-binding protein) in human endothelial cells, or by repressing HDAC6 thereby promoting α-tubulin acetylation in human adipose tissue-derived MSCs.[42] In our study, MBVs from 3D aggregates showed much higher miR-21 and miR-22 levels, probably due to the 3D culture microenvironment. Cells in 2D only endure mechanical response from the planar surface, while cells in 3D configurations have more contact resistance from other cells as well as the ECM.[43]

miR-125b has been reported to be an adhesion-regulated miRNA, and high seeding density or cell suspension or knockdown of beta5 integrin increased its expression.[44] In our study, the miR-125b from 3D MBVs was tenfold more abundant compared to 2D MBVs, which is consistent with the results in 2D versus 3D MSCs (approximately six- to seven-fold).[44] miR-125b protected MSCs from anoikis, prevented cell death in myocardial infarction, and reduced autophagic flux in infarcted hearts.[44,45] miR-21, -125b, and -145 played crucial roles in myofibroblast-suppressing and anti-scarring functions by inhibiting TGF-β2/SMAD2 pathway during wound healing.[10] Interestingly, miR-21 and miR-145 had distinct roles in regulating cancer cells, the former was a onco-miRNA, and the latter suppress tumorigenesis.[46] miR-155 was demonstrated to enhance the activation of Wnt/β-catenin pathway in glioma by suppressing the expression of HMG-box transcription factor 1, a strong Wnt pathway inhibitor; or to directly upregulated β-catenin at the transcriptional level.[47] Likewise, miR-221 promotes Wnt/β-catenin signaling as well by targeting DKK2.[48] Wnt/β-catenin pathway was well-known for activities such as cerebral cortical patterning in regulating rostral-caudal and medial-lateral patterning, radial inside to outside organization, and blood–brain barrier development.[49] In addition, miR-155 and miR-221 were involved in neural activities directly: miR-155 regulated neuroinflammation as a pro-inflammatory mediator, and miR-221 promoted neuronal differentiation and survival.[50]

It is recently recognized that EVs have promising therapeutic potential. As a new category of nanovesicles, MBVs were expected to be beneficial and play important roles in the ECM-tissue interface. This study evaluated the functional effects of

MBVs in vitro in several different culture models. In the forebrain organoid starvation model, iNPC aggregates were starved for 8 h in a nutrient-depleted medium and were recovered in a nutrient medium overnight with MBVs. Both 2D and 3D MBVs improved the cellular viability after recovery, indicating that MBVs were favorable to cells under stressed conditions such as starvation. Our results were consistent with the starved INS-1E β cells model treated with adipocyte-derived SuEVs, in which cells showed increased survival.[51] In the wound healing assay, neither 2D MBVs nor 3D MBVs facilitated wound closure, indicating that they did not promote fibroblast migration, which is different from SuEV effect on fibroblast migration,[52] especially the 3D SuEVs performed better than the 2D SuEVs.[11,23] In the proliferation assay, both 2D and 3D MBVs increased fibroblast growth in the first 2 days, which is consistent with another study,[52] but at a different temporal pattern. In our previous study, 3D SuEVs outperformed 2D SuEVs in several aspects, for example, stimulating expansion, reducing ROS, and rejuvenating senescent cells.[11] To explain functional differences between 2D and 3D MBVs, and between SuEVs and MBVs, further studies revealing the MBV cargos, such as miRNA sequencing and proteomics, are necessary.

Recently, increasing evidence suggests that EVs play a crucial role in immunomodulation, regulating both the activation and inhibition of the immune response. MSC-derived SuEVs have demonstrated their ability in reducing pro-inflammatory cytokines such as TNF-α, IL-1β, and IL-6, and promoteing anti-inflammatory cytokines such as IL-10 and TGF-β.[53] In splenocytes stimulated with anti-CD3/CD28, SuEVs produced from 3D hMSCs were shown to more efficiently reduce the release of pro-inflammatory cytokines and increase the secretion of immunoregulatory cytokines.[54] When regulating macrophages, hMSC-derived SuEVs suppressed M1 polarization and enhanced M2 polarization.[55] In our study, when treating macrophage with Aβ42 to stimulate an M1 phenotype, 2D MBVs reduced IL-12β, and 3D MBVs enhanced IL-10 at the mRNA level, indicating that 2D MBVs tended to attenuate the inflammation, while 3D MBVs preferred to augment anti-inflammatory effects. The most possible reason for this observation lies in the difference in mechanical, chemical, and topographical properties of 2D and 3D ECM,[43] since MBVs capture some of the properties of ECM. Another possible reason is the miRNAs, for instance, miR-21 and miR-155, participating in immunomodulation.[54,56] Moreover, variations in other cargo such as the non-coding Y RNAs (83–112 nucleotides) provide additional explanation, because Y RNAs regulate macrophage polarization via cytokine IL-10.[57] In addition, different signaling pathways being activated could lead to the difference. For example, SuEVs from ASCs suppressed the activation of M1 macrophages by targeting XNIP/NLRP3 pathway, while SuEVs from MSCs promoted M2 macrophage polarization potentially by the JAK1/STAT1/STAT6 signaling pathway.[58]

4. Conclusion

In this study, small RNA sequencing of 2D and 3D hMSCs revealed differences in signaling pathways and gene functions. MBVs were isolated from decellularized 2D and 3D hMSC-ECM. Different enzymes did not significantly influence the MBVs released from ECM. MBVs showed smaller sizes than SuEVs, and the concentrations and purities were lower than SuEVs. MBVs had a similar morphology as SuEVs but lack some exosomal markers. Some miRNAs were highly expressed in 3D MBVs rather than 2D MBVs. In vitro functional assay demonstrated that MBVs recovered the starved iNPCs and promoted fibroblast proliferation. When stimulated by Aβ42, 2D MBVs exhibited reduced pro-inflammatory factors, while 3D MBVs displayed an enhanced anti-inflammatory effect. This study has significance in advancing our understanding of the bio-interface of nanovesicles with human tissue and the design of cell-free-based therapy for treating neurological disorders such as Alzheimer's disease and ischemic stroke.

5. Experimental Section

hMSC Culture (2D-N, 2D-H, 3D) for EV Isolation: hMSCs between passages 0 and 2 were provided by the Tulane Center for Gene Therapy. The hMSCs were isolated from the bone marrow of multiple de-identified healthy donors (named as 7038, 7051, and 7052) aged 19–49 years old (Figure S1, Supporting Information). hMSCs (1×10^6 cells/mL/vial) in freezing media containing α-MEM, 2 mM L-glutamine, 30% fetal bovine serum (FBS), and 5% dimethyl sulfoxide (DMSO) were thawed and cultured following the method described in prior publications.[59] Briefly, 2D normoxia hMSCs were seeded at a density of 2000–2500 cells cm^{-2}, expanded and maintained in complete culture media (CCM) containing α-MEM with 10% FBS (Atlanta Biologicals, Lawrenceville, GA) and 1% penicillin/streptomycin (Life Technologies, Carlsbad, CA) in a standard incubator at 37 °C with 5% CO_2 and 20% O_2. For hypoxia 2D culture, hMSCs were incubated under hypoxia (2% O_2) in an oxygen-controlled chamber (BioSpherix, Ltd, NY). Cells were harvested when reaching 70–80% confluence by incubation with 0.25% trypsin/ethylenediaminetetraacetic acid (EDTA) (Invitrogen, Grand Island, NY) at 37 °C for 5–7 min. Harvested cells were re-plated and sub-cultured up to passage 4–6.

hMSC 3D dynamic culture as aggregates was carried out as previously reported.[24,60] Briefly, hMSCs at passages 4–6 were suspended in CCM (made of EV-depleted FBS), and were seeded at a density of 2.5×10^5 hMSCs/well in 3.0 mL media in ultra-low attachment (ULA) six-well plates (Corning). The ULA plates were then placed on a rocker (VWR International, PA) in a standard humidified incubator (37 °C, 5% CO_2) under controlled rocking angles of 9° and rocking speedof 20 rpm for 48 h.

miRNA Isolation and Library Construction: Cell samples from 2D and 3D hMSC cultures were collected. miRNA was isolated using RNeasy Mini Kit (QIAGEN, Germantown, MD, USA, 74104) according to manufacturer's instructions. CDNA library was constructed following the manual from QIAseq miRNA Library Kit and QIAseq miRNA 48 Index IL (QIAGEN, Germantown, MD, USA, 331505 and 331595). The quality, quantity, and average size of the cDNA library were measured via High Sensitivity DNA ScreenTape analysis (Agilent Technologies, Santa Clara, CA, USA, 5067-4626) and KAPA Library Quantification Kit (Kapa Biosystems, Wilmington, MA, USA, KR0405). Pooled samples were then subjected to RNA-sequencing on a NovaSeq 6000 sequencer (Illumina, San Diego, CA, USA) following NovaSeqXP workflow running single-end 100 cycles in a SP flow lane.

miRNA-Seq Data Analysis: Raw data were then demultiplexed and mapped into genome. The normalization through trimmed mean of M-values was performed on the gene counts data in ExpressAnalyst 4.2.2 following the filtration of unannotated genes and those with counts less than 4 and variance less than 15%. Limma was then used to identify DEGs. Heatmap and volcano plot were generated in this webtool. The functional mRNA targets of upregulated miRNAs or downregulated miRNAs were first identified in miRDB and the corresponding enrichment analysis was then performed through KEGG and GO (Biological Process, Cellular Component, Molecular Function), separately.

SuEV Isolation from Conditioned Media: For SuEV collection, the CCM was replaced with the media that contain EV-depleted FBS, and hMSCs were cultured for 48 h before media collection. To obtain EV-depleted FBS, the FBS was ultracentrifuged at 29 000 × *g* for 20 h at 4 °C. Differential ultracentrifugation combined with an inexpensive polyethylene glycol (PEG)-based method was used to isolate the SuEVs from the conditioned media.[23,61] Briefly, the conditioned media were centrifuged at 500 × *g* for 5 min (Eppendorf, Centrifuge 5810 R, Germany). The supernatants were centrifuged again at 2000 × *g* for 10 min. The collected supernatants were then centrifuged at 10 000 × *g* for 30 min. Then, supernatants were mixed with PEG solution (24% wt/vol in 1.5 M NaCl) at a 2:1 volume and incubated at 4 °C overnight. The solutions were centrifuged at 3214 × *g* for 60 min. The crude SuEV pellets were resuspended in 1 mL of phosphate buffered saline (PBS) and then ultracentrifuged (Beckman Coulter, Optima MAX-XP Ultracentrifuge, CA) at 100 000 × *g* for 70 min. Purified SuEV pellets were suspended in 100 µL PBS and shaken (Eppendorf, ThermoMixer C, Germany) for 15 min under 1500 rpm.

Decellularization for MBV Isolation: For 2D cells, the cultures were washed with PBS and decellularized using 0.5% Triton X-100 for 5 min,[62] then rinsed once with Hanks' balanced salt solution and once with ultrapure H_2O.[34] The cultures were then treated with ECM harvesting solution (50 mM tris [pH 7.5–8], 5 mM $CaCl_2$, and 200 mM NaCl) containing enzymes (collagenase at 0.01 mg mL^{-1}, or Proteinase K at 0.01 mg mL^{-1}) at 37 °C for 1 h to release MBVs from ECM.[31] The collected solution was used for MBV isolation. Briefly, samples were sequentially centrifuged at 500 × *g*, 2000 × *g*, and 10 000 × *g*, then were passed through 0.22 µm filters. After that, the MBV isolation procedure was the same as the SuEV isolation procedure. The 3D hMSC cultures were processed similarly to 2D cultures, except that after adding each solution, the samples were centrifuged at 500 × *g* for 5 min. Besides, the 3D samples were suspended in ultra-pure H_2O for 15 min before serial centrifugation.

Nanoparticle Tracking Analysis: NTA was performed on the isolated SuEVs and MBVs to determine particle size distribution and concentration, using Nanosight LM10-HS instrument (Malvern Instruments, Malvern, UK). It was configured with a blue laser (488 nm) and sCMOS camera. The samples were diluted as 1:1000 in filtered PBS. Three videos of 60 s were captured with camera shutter speed fixed at 30.00 ms. The camera level was set to 13, and the detection threshold was set to 5. Between each sample reading, the laser chamber was cleaned thoroughly with particle-free Milli-Q. The collected videos were analyzed using NTA3.4 software to obtain the mode and mean size distributions, as well as the concentration of particles.

Transmission Electron Microscopy: Electron microscopy imaging was used to confirm the morphology and size of SuEVs and MBVs as shown in the authors' previous studies.[63,64] Briefly, SuEV and MBV isolates were resuspended in 30 µL of filtered PBS. For each sample preparation, intact SuEVs and MBVs (15 µL) were dropped onto Parafilm. A carbon-coated 400 Hex Mesh Copper grid (electron microscopy sciences, EMS) was positioned using forceps with coating side down on top of each drop for 1 h. Grids were rinsed three times with 30 µL filtered PBS before being fixed in 2% paraformaldehyde (PFA) for 10 min (EMS, EM Grade). The grids were then transferred on top of a 20 µL drop of 2.5% glutaraldehyde (EMS, EM Grade) and incubated for 10 min. Samples were stained for 10 min with 2% uranyl acetate (EMS grade). Then the samples were embedded for 10 min with a mixture of 0.13% methyl cellulose and 0.4% uranyl acetate. The coated side of the grids were left to dry before imaging on the TEM HT7800 (Hitachi, Janan). Image analysis was performed using ImageJ software to determine the average sizes of SuEVs and MBVs.

DNA Assay: DNA assay was used to assess nuclei content before and after decellularization. Before decellularization, the cells were dissociated with trypsin into single cells. After decellularization, the cells were either treated with DNase I (2000 U mL^{-1}) before DNA assay, or performed the assay directly as described previously.[62] A series of DNA standards were prepared by dissolving salmon testes DNA in TEX (10 mM Tris, 1 mM EDTA, 0.1% Triton X-100 at pH 8) and a standard curve was constructed for each assay. The samples were lysed overnight with 0.1 mg mL^{-1} proteinase K (Sigma-Aldrich, St. Louis, MO) overnight at 50 °C. The lysates (100 µL) were placed into a 96-well plate and were mixed with 100 µL of Picogreen (Molecular Probes, Eugene, OR). The plate was incubated for 5 min and then read on a fluorescent plate reader with 485ex/528em (Bio-Rad Laboratories, Hercules, CA).

Immunocytochemistry: To observe the ECM component after decellularization, the samples were fixed with 4% PFA for 1 h, and then were blocked with blocking buffer (5% FBS in PBS) for 30 min. After that, the samples were incubated with primary antibodies Laminin (rabbit IgG, 1:100, Abcam Inc., Eugene, OR) and Collagen I (rabbit IgG, 1:100, Abcam Inc.) at 4 °C overnight and then were stained with secondary antibody Alexa Fluor 488 goat anti-rabbit IgG (1:200, Invitrogen) for 1 h at room temperature. To observe the nuclei, the samples were stained with Hoechst 33342 (1:2000, Invitrogen) for 3 min at room temperature. The samples were imaged using a fluorescent microscope (Olympus IX70, Melville, NY).

Western Blot: SuEV and MBV samples were lysed in radioimmunoprecipitation assay buffer (150 mM sodium chloride, 1.0% Trition X-100, 0.5% sodium deoxycholate, 0.1% sodium dodecyl sulfate, 50 mM tris, pH 8, 2 µg mL^{-1} aprotinin, 5 µg mL^{-1} leupeptin, 5 µg mL^{-1} antipain, 1 mM PMSF protease inhibitor) together with 1% of proteinase inhibitor cocktails (Invitrogen) for 20 min on ice, and spun down at 14000 rpm for 20 min. The supernatant was collected, and protein concentration was determined by a Bradford assay. Protein lysate concentrations were normalized, and 20 µg of each sample was denatured at 95 °C in 2× Laemmli Sample buffer. Proteins were loaded into 12% BIS-Tris-SDS gels and transferred onto a nitrocellulose membrane (Bio-rad). The membranes were then blocked for 1 h in 5% skim milk (w/v) in Tris-buffered saline (10 mM Tris-HCl, pH 7.5, and 150 mM NaCl) with 0.1% Tween 20 (v/v) (TBST). Membranes were incubated overnight in the presence of the primary antibodies (Table S2, Supporting Information) diluted in the blocking buffer at 4 °C. Afterward, the membranes were washed four times with TBST for 10 min each time and then incubated with an IR secondary (LI-COR, Lincoln, NE) at 1:5000 for 90 min at room temperature. The blots were then washed four more times with TBST for 10 min each time before being processed with the LI-COR Odyssey (LI-COR Biosciences).

miRNA and mRNA Analysis by Reverse Transcription Polymerase Chain Reaction: Total miRNA was isolated from different MBV samples using the TRIzol LS Reagent (Invitrogen, Waltham, MA) according to the manufacturer's protocol. The commercial qScript miR cDNA synthesis kit was used for reverse transcription (Quantabio, Beverly, MA). The PerfeCTa Universal PCR Primer (Quantabio) was designed and validated to work specifically with PerfeCTa SYBR Green SuperMix using miRNA cDNA produced. The tested miRNA primer sequences are shown in Table S3, Supporting Information. Real-time RT-PCR were performed on an Applied Biosystems Quantstudio 7 flex (Applied Biosystems, Foster City, CA), using SYBR1 Green PCR Master Mix (Applied Biosystems). The reactions were performed as follows: 10 min at 95 °C to denature, and 40 cycles of 95 °C for 15 s and 60 °C for 30 s, and 70 °C for 30 s. Fold variation in gene expression was quantified by the delta–delta Ct approach: $2^{-(\Delta C_{t\ \text{treatment}} - \Delta C_{t\ \text{control}})}$, which was based on the comparison of the target gene (normalized to SNORD44) between the compared samples.

Total mRNA was isolated using the RNeasy Plus kit (Qiagen, Hilden, Germany) following vendor's instructions. Reverse transcription was carried out using 2 µg of total RNA, anchored oligo-dT primers (Operon) and Superscript III (Invitrogen). Primers were designed using the software Oligo Explorer 1.2 (Genelink) (Table S4, Supporting Information). RT-PCR reactions were performed on an ABI7500 instrument (Applied Biosystems), using SYBR Green PCR Master Mix. Fold variations in gene expressions were quantified using the delta–delta Ct approach: $2^{-(\Delta C_{t\ \text{treatment}} - \Delta C_{t\ \text{control}})}$, which was based on the comparison of the target gene (normalized to β-actin) among different conditions.

In Vitro Wound Healing Model and the Fibroblast Proliferation Model: Primary human dermal fibroblasts (hFBs) were purchased from American Type Culture Collection (ATCC, PCS-201-012; Manassas, VA, USA) and sub-cultured up to passage 15. In vitro wound healing assay was modified to evaluate the effects of MBVs.[11,23] Briefly, hFBs were seeded (1×10^5 cell/per well) onto a tissue culture treated 24-well plate and grown for 48 h in DMEM plus 10% FBS. MBVs then were added at the

concentration 1×10^9 MBV mL^{-1} medium. An artificial wound was introduced with a 200 µL pipette tip and images were captured with an Olympus IX70 inverted microscope for 0–16 h. For the proliferation assay, hFBs were seeded (5000 cells/per well) onto a tissue culture treated 24-well plate and grown for 96 h in DMEM plus 10% FBS. MBVs were added at the concentration of 1.69×10^8 MBV mL^{-1}. The cell counting was performed every 24 h. Each assay was performed with triplicates.

In Vitro Forebrain Organoid Starvation Model: Forebrain organoids composed of neural progenitor cells (iNPCos) were differentiated from human induced pluripotent stem cells (iPSCs) as reported in the authors' previous studies.[64,65] Undifferentiated human iPSCs were seeded into ULA 96-well plates (Corning Inc., New York, NY) at 1×10^5 cells/well in differentiation medium composed of DMEM/F-12 plus 2% B27 serum-free supplement (Life Technologies, Carlsbad, CA), in the presence of Y27632 (10 µM). After 24 h, Y27632 was removed and the cells were treated with dual SMAD signaling inhibitors of 10 µM SB431542 (Sigma-Aldrich, St. Louis, MO) and 100 nM LDN193189 (Sigma) over 7 days. Then the iNPC spheroids were starved by switching to DMEM/F12 without B27 for 0, 4, and 8 h. The spheroids were then recovered by switching to DMEM/F-12 plus B27 overnight. At the same time, MBVs were added at a concentration of 1×10^8 MBV/well. After recovery, the MTT assay was performed to determine the viability of the spheroids. Briefly, 100 µL of 5 mg mL^{-1} MTT solution was added to 100 µL of culture medium. The cultures were incubated at 37 °C for 3 h. Then, the formazan crystals were centrifuged and hydrolyzed by DMSO. Afterward, the pink solution was read at 570 nm by the microplate reader (BioRad Laboratories, Hercules, CA).

In Vitro Macrophage Polarization Model: THP-1 cells were obtained from ATTC and cultured in ATCC-formulated RPMI-1640 until confluency. THP-1 cells were passaged into 24-well plates at a concentration of 1×10^5 cells/well. THP-1 cells were then differentiated into macrophages (M0) by a 48-h treatment of phorbol 12-myristate 13-acetate (PMA, 20 nM, Sigma) in RPMI-1640, as reported in the authors' previous study.[25] M0 macrophages were then polarized into the M1 phenotype with 24 h-treatment of amyloid beta (Aβ)42 oligomers (0.4 µM, Sigma) or the M2 phenotype with a 24-h treatment of IL-4 (10 ng mL^{-1}, Peprotech). MBVs were added to the culture at the concentration of 1×10^8 particles mL^{-1} at the beginning of polarization. M1 or M2 polarization markers were tested by RT-PCR and ELISA assays were performed for the secreted cytokines.

The Enzyme-Linked Immunosorbent Assay: ELISA assay was employed for determining the secreted cytokines TNF-α, IL-6, and IL-1β. Macrophage culture supernatants were collected at 24 h after adding stimulations. Concentrations of cytokines were measured according to the manufacturers' instructions (BioLegend, San Diego, CA). Briefly, the capture antibodies were incubated in 96-well microplates overnight at 4 °C. The next day, non-specific binding was blocked for 1 h at room temperature, then the samples and standards were added and incubated overnight at 4 °C. Then, detection antibodies were added and incubated at room temperature for 1 h. Next, Avidin-horseradish peroxidase solution was added for 30 min, followed by 3,3′,5,5′-tetramethylbenzidine substrate solution for 15 min. Then the reaction was stopped by the stop solution. The absorbance was measured using a microplate reader (Bio-Rad, Richmond, CA) at a wavelength of 450 nm. All cytokine samples were run in triplicate.

Statistical Analysis: All experiments were performed in triplicate ($n = 3$), and representative data were reported. Experimental results were expressed as means ± standard deviation (SD). Statistical comparisons were performed by one-way ANOVA and Tukey's post hoc test for multiple comparisons, and significance was accepted at $p < 0.05$. For comparisons of two conditions, student's *t*-test was performed for the statistical analysis.

Supporting Information

Supporting Information is available from the Wiley Online Library or from the author.

Acknowledgements

The authors would like to thank Dr. Brian K. Washburn at Florida State University (FSU) Department of Biological Sciences for their help with RT-PCR analysis, and Dr. Bruce Bunnell at University of North Texas for providing bone marrow hMSCs. The Hitachi HT7800 for TEM was funded from NSF grant 2017869. Research reported in this publication was supported by the National Institutes of Health (USA) under Award Number R01NS125016. The content is solely the responsibility of the authors and does not necessarily represent the official views of the National Institutes of Health.

Conflict of Interest

The authors declare no conflict of interest.

Author Contributions

C.L. did the majority of the work and wrote the manuscript. X.C. facilitated the experiments. Yu.L. performed miRNA sequencing. L.S. helped C.L. with EV characterizations. Z.Y., R.Y., and C.Z. participated in the discussion and manuscript review. Ya.L. perceived the experiments, wrote, revised, and finalized the manuscript.

Data Availability Statement

The data that support the findings of this study are available from the corresponding author upon reasonable request.

Keywords

extracellular matrices, extracellular vesicles, human mesenchymal stem cells, matrix-found nanovesicles, three-dimensional aggregates

Received: April 8, 2023
Revised: May 19, 2023
Published online:

[1] L. d. S. Meirelles, P. C. Chagastelles, N. B. Nardi, *J. Cell Sci.* **2006**, *119*, 2204.
[2] D. E. Rodríguez-Fuentes, L. E. Fernández-Garza, J. A. Samia-Meza, S. A. Barrera-Barrera, A. I. Caplan, H. A. Barrera-Saldaña, *Arch. Med. Res.* **2021**, *52*, 93.
[3] J. Galipeau, L. Sensébé, *Cell Stem Cell* **2018**, *22*, 824.
[4] M. E. Bernardo, W. E. Fibbe, *Ann. N. Y. Acad. Sci.* **2012**, *1266*, 107.
[5] J. Galipeau, M. Krampera, K. Leblanc, J. A. Nolta, D. G. Phinney, Y. Shi, K. Tarte, S. Viswanathan, I. Martin, *Cytotherapy* **2021**, *23*, 368.
[6] a) M. Kabat, I. Bobkov, S. Kumar, M. Grumet, *Stem Cells Transl. Med.* **2020**, *9*, 17; b) T. Squillaro, G. Peluso, U. Galderisi, *Cell Transplant.* **2016**, *25*, 829; c) X. Wei, X. Yang, Z.-p. Han, F.-f. Qu, L. Shao, Y.-f. Shi, *Acta Pharmacol. Sin.* **2013**, *34*, 747; d) X.-L. Fan, Y. Zhang, X. Li, Q.-L. Fu, *Cell. Mol. Life Sci.* **2020**, *77*, 2771.
[7] a) L. Timmers, S. K. Lim, F. Arslan, J. S. Armstrong, I. E. Hoefer, P. A. Doevendans, J. J. Piek, R. M. El Oakley, A. Choo, C. N. Lee, *Stem Cell Res.* **2008**, *1*, 129; b) L. Timmers, S. K. Lim, I. E. Hoefer, F. Arslan, R. C. Lai, A. A. van Oorschot, M. J. Goumans, C. Strijder, S. K. Sze, A. Choo, *Stem Cell Res.* **2011**, *6*, 206; c) N. Bogatcheva, M. Coleman, *Biochemistry* **2019**, *84*, 1375.
[8] S. Öztürk, A. E. Elçin, A. Koca, Y. M. Elçin, *Stem Cell Rev Rep* **2021**, *17*, 390.

[9] a) R. C. Lai, F. Arslan, M. M. Lee, N. S. K. Sze, A. Choo, T. S. Chen, M. Salto-Tellez, L. Timmers, C. N. Lee, R. M. El Oakley, *Stem Cell Res.* **2010**, *4*, 214; b) Y. Nakamura, S. Miyaki, H. Ishitobi, S. Matsuyama, T. Nakasa, N. Kamei, T. Akimoto, Y. Higashi, M. Ochi, *FEBS Lett.* **2015**, *589*, 1257; c) X. H. Gong, H. Liu, S. J. Wang, S. W. Liang, G. G. Wang, *J. Cell. Physiol.* **2019**, *234*, 13878.
[10] S. Fang, C. Xu, Y. Zhang, C. Xue, C. Yang, H. Bi, X. Qian, M. Wu, K. Ji, Y. Zhao, *Stem Cells Transl. Med.* **2016**, *5*, 1425.
[11] X. Yuan, L. Sun, R. Jeske, D. Nkosi, S. B. York, Y. Liu, S. C. Grant, D. G. Meckes Jr, Y. Li, *J Extracell Vesicles* **2022**, *11*, e12235.
[12] V. Bodart-Santos, L. R. de Carvalho, M. A. de Godoy, A. F. Batista, L. M. Saraiva, L. G. Lima, C. A. Abreu, F. G. De Felice, A. Galina, R. Mendez-Otero, *Stem Cell Res. Ther.* **2019**, *10*, 332.
[13] a) X. Zhang, E. G. Borg, A. M. Liaci, H. R. Vos, W. Stoorvogel, *J Extracell Vesicles* **2020**, *9*, 1791450; b) F. Royo, C. Théry, J. M. Falcón-Pérez, R. Nieuwland, K. W. Witwer, *Cells* **2020**, *9*, 1955; c) L. Dong, R. C. Zieren, K. Horie, C. J. Kim, E. Mallick, Y. Jing, M. Feng, M. D. Kuczler, J. Green, S. R. Amend, *J Extracell Vesicles* **2020**, *10*, e12044.
[14] L. Huleihel, G. S. Hussey, J. D. Naranjo, L. Zhang, J. L. Dziki, N. J. Turner, D. B. Stolz, S. F. Badylak, *Sci. Adv.* **2016**, *2*, e1600502.
[15] a) A. Sainio, H. Järveläinen, *Cell Signal* **2020**, *66*, 109487; b) C. Frantz, K. M. Stewart, V. M. Weaver, *J. Cell Sci.* **2010**, *123*, 4195; c) M. Mongiat, E. Andreuzzi, G. Tarticchio, A. Paulitti, *Int. J. Mol. Sci.* **2016**, *17*, 1822; d) J. L. Dziki, L. Huleihel, M. E. Scarritt, S. F. Badylak, *Tissue Eng., Part A* **2017**, *23*, 1152; e) L. Sorokin, *Nat. Rev. Immunol.* **2010**, *10*, 712.
[16] L. Huleihel, J. G. Bartolacci, J. L. Dziki, T. Vorobyov, B. Arnold, M. E. Scarritt, C. P. Molina, S. T. LoPresti, B. N. Brown, J. D. Naranjo, *Tissue Eng., Part A* **2017**, *23*, 1283.
[17] a) Y. Van der Merwe, A. E. Faust, M. B. Steketee, *Neural Regen Res* **2017**, *12*, 1597; b) A. Faust, A. Kandakatla, Y. van der Merwe, T. Ren, L. Huleihel, G. Hussey, J. D. Naranjo, S. Johnson, S. Badylak, M. Steketee, *J. Biomater. Appl.* **2017**, *31*, 1277.
[18] Y. van der Merwe, A. E. Faust, E. T. Sakalli, C. C. Westrick, G. Hussey, K. C. Chan, I. P. Conner, V. L. Fu, S. F. Badylak, M. B. Steketee, *Sci. Rep.* **2019**, *9*, 3482.
[19] R. J. Crum, K. Hall, C. P. Molina, G. S. Hussey, E. Graham, H. Li, S. F. Badylak, *NPJ Regener. Med.* **2022**, *7*, 13.
[20] C. Mora-Navarro, A. Badileanu, A. M. G. Martins, E. W. Ozpinar, L. Gaffney, I. Huntress, E. Harrell, J. R. Enders, X. Peng, R. C. Branski, *ACS Biomater Sci Eng* **2020**, *6*, 1690.
[21] G. Ronan, G. Bahcecioglu, J. Yang, P. Zorlutuna, *bioRxiv* **2022**, https://doi.org/10.1101/2022.11.14.516464.
[22] S. C. Santos, C. A. Custódio, J. F. Mano, *Adv. Healthcare Mater.* **2022**, *11*, 2102383.
[23] R. Jeske, C. Liu, L. Duke, M. L. C. Castro, L. Muok, P. Arthur, M. Singh, S. Jung, L. Sun, Y. Li, *Bioact. Mater.* **2022**, *25*, 732.
[24] a) X. Yuan, J. T. Rosenberg, Y. Liu, S. C. Grant, T. Ma, *Cytotherapy* **2019**, *21*, 1033; b) B. M. Bijonowski, X. Yuan, R. Jeske, Y. Li, S. C. Grant, *Sci. Rep.* **2020**, *10*, 20448.
[25] X. Yuan, L. Sun, R. Jeske, D. Nkosi, S. York, Y. Liu, S. C. Grant, D. G. J. Meckes, Y. Li, *J Extracell Vesicles* **2022**, *11*, e12235.
[26] a) B. M. Bijonowski, Q. Fu, X. Yuan, J. Irianto, Y. Li, S. C. Grant, T. Ma, *Biotechnol. Bioeng.* **2020**, *117*, 3136; b) S. Sart, A.-C. Tsai, Y. Li, T. Ma, *Tissue Eng Part B Rev* **2014**, *20*, 365.
[27] M. Marzano, J. Bejoy, M. R. Cheerathodi, L. Sun, S. B. York, J. Zhao, T. Kanekiyo, G. Bu, D. G. Meckes Jr, Y. Li, *Cells* **2019**, *8*, 993.
[28] a) L.-L. Lv, Y. Cao, D. Liu, M. Xu, H. Liu, R.-N. Tang, K.-L. Ma, B.-C. Liu, *Int. J. Biol. Sci.* **2013**, *9*, 1021; b) E. Trenkenschuh, M. Richter, E. Heinrich, M. Koch, G. Fuhrmann, W. Friess, *Adv. Healthcare Mater.* **2022**, *11*, 2100538; c) E. Schulz, A. Karagianni, M. Koch, G. Fuhrmann, *Eur. J. Pharm. Biopharm.* **2020**, *146*, 55; d) J.-J. Ban, M. Lee, W. Im, M. Kim, *Biochem. Biophys. Res. Commun.* **2015**, *461*, 76.
[29] a) G. S. Hussey, J. L. Dziki, Y. C. Lee, J. G. Bartolacci, M. Behun, H. R. Turnquist, S. F. Badylak, *J Immunol Regen Med* **2019**, *3*, 26; b) R. J. Crum, H. Capella-Monsonís, J. Chang, M. J. Dewey, B. D. Kolich, K. T. Hall, S. O. El-Mossier, D. G. Nascari, G. S. Hussey, S. F. Badylak, *Acta Biomater.* **2022**, *155*, 113; c) N. J. Turner, L. M. Quijano, G. S. Hussey, P. Jiang, S. F. Badylak, *Tissue Eng., Part A* **2022**, *28*, 879.
[30] E. Linetsky, R. Bottino, R. Lehmann, R. Alejandro, L. Inverardi, C. Ricordi, *Diabetes* **1997**, *46*, 1120.
[31] L. M. Quijano, J. D. Naranjo, S. O. El-Mossier, N. J. Turner, C. P. Molina, J. Bartolacci, L. Zhang, L. White, H. Li, S. F. Badylak, *Tissue Eng., Part C* **2020**, *26*, 528.
[32] a) E. Serrano-Pertierra, M. Oliveira-Rodríguez, M. Rivas, P. Oliva, J. Villafani, A. Navarro, M. C. Blanco-López, E. Cernuda-Morollón, *Bioengineering* **2019**, *6*, 8; b) L. Min, S. Zhu, L. Chen, X. Liu, R. Wei, L. Zhao, Y. Yang, Z. Zhang, G. Kong, P. Li, *J Extracell Vesicles* **2019**, *8*, 1643670.
[33] C. Charoenviriyakul, Y. Takahashi, M. Morishita, M. Nishikawa, Y. Takakura, *Mol. Pharmaceutics* **2018**, *15*, 1073.
[34] G. S. Hussey, C. P. Molina, M. C. Cramer, Y. Y. Tyurina, V. A. Tyurin, Y. C. Lee, S. O. El-Mossier, M. H. Murdock, P. S. Timashev, V. E. Kagan, *Sci. Adv.* **2020**, *6*, eaay4361.
[35] a) J. Zhang, S. Li, L. Li, M. Li, C. Guo, J. Yao, S. Mi, *Genomics, Proteomics Bioinf.* **2015**, *13*, 17; b) S. Sart, X. Yuan, R. Jeske, Y. Li, *Molecular Players in iPSC Technology*, Advances in Stem Cell Biology, Vol. *1*, Elsevier, **2022**.
[36] a) D. Hassel, P. Cheng, M. P. White, K. N. Ivey, J. Kroll, H. G. Augustin, H. A. Katus, D. Y. Stainier, D. Srivastava, *Circ. Res.* **2012**, *111*, 1421; b) X. Wang, C. C. Ling, L. Li, Y. Qin, J. Qi, X. Liu, B. You, Y. Shi, J. Zhang, Q. Jiang, *Cardiovasc Res* **2016**, *110*, 140.
[37] J. Dong, Z. Zhang, H. Huang, P. Mo, C. Cheng, J. Liu, W. Huang, C. Tian, C. Zhang, J. Li, *Stem Cell Res. Ther.* **2018**, *9*, 151.
[38] C. Gollmann-Tepeköylü, L. Pölzl, M. Graber, J. Hirsch, F. Nägele, D. Lobenwein, M. W. Hess, M. J. Blumer, E. Kirchmair, J. Zipperle, *Cardiovasc. Res.* **2020**, *116*, 1226.
[39] L. Gou, C. Xue, X. Tang, Z. Fang, *Aging* **2020**, *12*, 23609.
[40] a) S. Taverna, S. Fontana, F. Monteleone, M. Pucci, L. Saieva, V. De Caro, V. G. Cardinale, M. Giallombardo, E. Vicario, C. Rolfo, *OncoTargets Ther.* **2016**, *7*, 30420; b) C. Tan, F. Jia, P. Zhang, X. Sun, Y. Qiao, X. Chen, Y. Wang, J. Chen, Y. Lei, *J. Mater. Chem. B* **2021**, *9*, 3335.
[41] C. X. Li, N. P. Talele, S. Boo, A. Koehler, E. Knee-Walden, J. L. Balestrini, P. Speight, A. Kapus, B. Hinz, *Nat. Mater.* **2017**, *16*, 379.
[42] a) Y. Feng, L. Wang, T. Wang, Y. Li, Q. Xun, R. Zhang, L. Liu, L. Li, W. Wang, Y. Tian, *Mol. Ther.* **2021**, *29*, 2151; b) S. Huang, S. Wang, C. Bian, Z. Yang, H. Zhou, Y. Zeng, H. Li, Q. Han, R. C. Zhao, *Stem Cells Dev.* **2012**, *21*, 2531; c) X. Wang, L. Wang, Y. Sun, B. Chen, L. Xiong, J. Chen, M. Huang, J. Wu, X. Tan, Y. Zheng, *Cell Proliferation* **2020**, *53*, e12911.
[43] K. Duval, H. Grover, L.-H. Han, Y. Mou, A. F. Pegoraro, J. Fredberg, Z. Chen, *Physiology* **2017**, *32*, 266.
[44] X. Yu, D. M. Cohen, C. S. Chen, *Stem Cells* **2012**, *30*, 956.
[45] a) L.-P. Zhu, T. Tian, J.-Y. Wang, J.-N. He, T. Chen, M. Pan, L. Xu, H.-x. Zhang, X.-T. Qiu, C.-C. Li, *Theranostics* **2018**, *8*, 6163; b) C. Xiao, K. Wang, Y. Xu, H. Hu, N. Zhang, Y. Wang, Z. Zhong, J. Zhao, Q. Li, D. Zhu, *Circ. Res.* **2018**, *123*, 564.
[46] a) Y. Yu, P. Nangia-Makker, L. Farhana, S. G. Rajendra, E. Levi, A. P. Majumdar, *Mol Cancer* **2015**, *14*, 98; b) M. Si, S. Zhu, H. Wu, Z. Lu, F. Wu, Y. Mo, *Oncogene* **2007**, *26*, 2799; c) J. Li, L. Wu, M. Pei, Y. Zhang, *J Ovarian Res* **2020**, *13*, 111.
[47] a) Z. Yan, S. Che, J. Wang, Y. Jiao, C. Wang, Q. Meng, *Tumour Biol* **2015**, *36*, 5323; b) N. Liu, F. Jiang, X. Han, M. Li, W. Chen, Q. Liu, C. Liao, Y. Lv, *Riv. Eur. Sci. Med. Farmacol.* **2018**, *22*, 101.
[48] a) Y. Wang, Y. Zhao, A. Herbst, T. Kalinski, J. Qin, X. Wang, Z. Jiang, F. Benedix, S. Franke, T. Wartman, *Ann Surg* **2016**, *264*, 804; b) Z. Chen,

T. Pan, D. Jiang, L. Jin, Y. Geng, X. Feng, A. Shen, L. Zhang, *Mol Ther Nucleic Acids* **2020**, *19*, 1434.

[49] a) A. Chenn, *Organogenesis* **2008**, *4*, 76; b) Y. Hirabayashi, Y. Itoh, H. Tabata, K. Nakajima, T. Akiyama, N. Masuyama, Y. Gotoh, Development **2004**, *131*, 2791; c) S. Liebner, M. Corada, T. Bangsow, J. Babbage, A. Taddei, C. J. Czupalla, M. Reis, A. Felici, H. Wolburg, M. Fruttiger, *J. Cell Biol.* **2008**, *183*, 409.

[50] a) V. D. Zingale, A. Gugliandolo, E. Mazzon, *Int. J. Mol. Sci.* **2021**, *23*, 90; b) S. H. Rastegar-Moghaddam, A. Ebrahimzadeh-Bideskan, S. Shahba, A. M. Malvandi, A. Mohammadipour, *Cell. Mol. Neurobiol.* **2022**, *43*, 455; c) N. Hamada, Y. Fujita, T. Kojima, A. Kitamoto, Y. Akao, Y. Nozawa, M. Ito, *Neurochem. Int.* **2012**, *60*, 743; d) S. E. Oh, H.-J. Park, L. He, C. Skibiel, E. Junn, M. M. Mouradian, *Redox Biol.* **2018**, *19*, 62.

[51] I. Gesmundo, B. Pardini, E. Gargantini, G. Gamba, G. Birolo, A. Fanciulli, D. Banfi, N. Congiusta, E. Favaro, M. C. Deregibus, *JCI Insight* **2021**, *6*, e141962.

[52] A. Casado-Díaz, J. M. Quesada-Gómez, G. Dorado, *Front. Bioeng. Biotechnol.* **2020**, *8*, 146.

[53] a) J. Zhang, Y. Rong, C. Luo, W. Cui, *Aging* **2020**, *12*, 25138; b) W. Zhou, M. Silva, C. Feng, S. Zhao, L. Liu, S. Li, J. Zhong, W. Zheng, *Stem Cell Res. Ther.* **2021**, *12*, 174.

[54] H. Kim, M. J. Lee, E.-H. Bae, J. S. Ryu, G. Kaur, H. J. Kim, J. Y. Kim, H. Barreda, S. Y. Jung, J. M. Choi, *Mol. Ther.* **2020**, *28*, 1628.

[55] G. R. Willis, A. Fernandez-Gonzalez, J. Anastas, S. H. Vitali, X. Liu, M. Ericsson, A. Kwong, S. A. Mitsialis, S. Kourembanas, *Am J. Respir. Crit. Care Med.* **2018**, *197*, 104.

[56] Y.-M. Pers, C. Bony, I. Duroux-Richard, L. Bernard, M. Maumus, S. Assou, F. Barry, C. Jorgensen, D. Noël, *Front. Immunol.* **2021**, *12*, 624024.

[57] L. Cambier, G. de Couto, A. Ibrahim, A. K. Echavez, J. Valle, W. Liu, M. Kreke, R. R. Smith, L. Marbán, E. Marbán, *EMBO Mol. Med.* **2017**, *9*, 337.

[58] a) Y. Liu, G. Lou, A. Li, T. Zhang, J. Qi, D. Ye, M. Zheng, Z. Chen, *EBioMedicine* **2018**, *36*, 140; b) L. Cao, H. Xu, G. Wang, M. Liu, D. Tian, Z. Yuan, *Int. Immunopharmacol.* **2019**, *72*, 264.

[59] A.-C. Tsai, Y. Liu, X. Yuan, T. Ma, *Tissue Eng., Part A* **2015**, *21*, 1705.

[60] A. C. Tsai, Y. Liu, X. Yuan, R. Chella, T. Ma, *Biotechnol. J.* **2017**, *12*, 1600448.

[61] R. Jeske, X. Chen, S. Ma, E. Z. Zeng, T. P. Driscoll, Y. Li, *Biochem. Eng. J.* **2022**, *188*, 108711.

[62] a) S. Sart, T. Ma, Y. Li, *Tissue Eng., Part A* **2014**, *20*, 54; b) S. Sart, Y. Yan, Y. Li, E. Lochner, C. Zeng, T. Ma, Y. Li, *Acta Biomater.* **2016**, *30*, 222; c) Y. Yan, L. Martin, D. Bosco, J. Bundy, R. Nowakowski, Q. X. Sang, Y. Li, *Biomaterials* **2015**, *73*, 231; d) S. Sart, R. Jeske, X. Chen, T. Ma, Y. Li, *Tissue Eng Part B Rev* **2020**, *26*, 402.

[63] M. Marzano, J. Bejoy, M. Cheerathodi, L. Sun, S. York, J. Zhao, T. Kanekiyo, G. Bu, D. G. Meckes Jr., Y. Li, *Cells* **2019**, *8*, 993.

[64] M. Marzano, M. J. Bou-Dargham, A. S. Cone, S. York, S. Helsper, S. C. Grant, D. G. Meckes Jr., Q. X. Sang, Y. Li, *ACS Biomater. Sci. Eng.* **2021**, *7*, 1111.

[65] a) Y. Yan, J. Bejoy, J. Xia, J. Guan, Y. Zhou, Y. Li, *Acta Biomater.* **2016**, *42*, 114; b) Y. Yan, L. Song, J. Madinya, T. Ma, Y. Li, *Tissue Eng., Part A* **2018**, *24*, 418; c) S. Helsper, Y. Yuan, F. A. Bagdasarian, A. Jacob, Y. Li, C. V. Borlongan, S. C. Grant, *Transl Stroke Res* **2022**, https://doi.org/10.1007/s12975-022-01057-w.